Int. J. Therm. Sci. (1999) 38, 585–594

Numerical hydrodynamic and thermal analysis of laminar flow in curved elliptic and rectangular ducts

Ricardo Junqueira Silva*, Ramón Molina Valle, Márcio Ziviani

Departamento de Engenharia Mecânica, Universidade Federal de Minas Gerais, Av. Antônio Carlos, 6627, Belo Horizonte, MG, 31270-010, Brazil

(Received 19 May 1998, accepted 21 December 1998)

Abstract — The complete forms of the Navier–Stokes and energy conservation equations are solved for a steady, fully developed, incompressible laminar flow with constant physical properties in ducts with elliptic or rectangular cross section. The equations are solved using the finite volume method with a boundary fitted coordinate system. The curvature ratio, which is included in the conservation equations, is kept constant. Solutions are obtained for several flow rates (Dean number between 30 and 400) and cross sections (ellipses and rectangles with aspect ratio between 0.7 and 1.4). The axial and secondary velocities and temperature profiles, the heat transfer and pressure drop are analysed. Results are compared with the literature for validation of the numerical approach. © Elsevier, Paris.

curved ducts / elliptical and rectangular ducts / forced convection / laminar flow / numerical analysis

Résumé — Analyse hydrodynamique et thermique par méthode numérique d'un écoulement laminaire dans des canalisations courbes à section rectangulaire ou elliptique. Les formes complètes des équations de Navier–Stokes et de la conservation de l'énergie sont résolues pour l'écoulement régulier, développé et laminaire d'un fluide incompressible, à propriétés physiques constantes, dans des canalisations à sections elliptiques ou rectangulaires. Les équations sont résolues en utilisant la méthode des volumes finis, avec un système de coordonnées généralisées, adaptées aux conditions aux limites géométriques. Le taux de courbure, qui est inclus dans les équations de bilan, est maintenu constant. Les résultats sont obtenus pour plusieurs débits (nombre de Dean compris entre 30 et 400) et plusieurs type de sections (elliptique et rectangulaire, ayant un rapport hauteur/largeur compris entre 0,7 et 1,4). Les profils de température et de vitesses axiale et normales sont analysés, ainsi que les transferts thermiques et les pertes de pression. Les résultats du modèle sont validés par comparaison avec des données issues de la littérature. © Elsevier, Paris.

canalisations courbes / sections elliptiques et rectangulaires / convection forcée / écoulement laminaire / modélisation

Nomenclature

a	rectangle width or horizontal ellipse semi-axis	m
a	coefficient in the discretized equation	
b	rectangle semi-height or vertical ellipse semi-axis	m
b	linearized source term	
c_p	specific heat	$kJ \cdot kg^{-1} \cdot K^{-1}$
f	friction factor	
J	Jacobian	
k	thermal conductivity	$W \cdot m^{-1} \cdot K^{-1}$
K	Dean number, $K = Re\sqrt{l/r_c}$	
l	characteristic length, $l = \sqrt{a\,b}$	m
Nu	Nusselt number, $Nu = hl/k$	
p	pressure	Pa
r	dimensionless radius, $r = x/a$ or $r = y/b$	
Re	Reynolds number, $Re = \rho\, l\, \overline{w}/\mu$	
r_c	curvature radius	m
S	source term	
T	temperature	°C
$\overline{T}$	mean temperature	°C
u, v, w	velocity components	$m \cdot s^{-1}$
U,V	contra-variant velocity components	$m \cdot s^{-1}$

* Correspondence and reprints.

x, y, z	coordinates in the physical plane	m
W	dimensionless axial velocity, $W = w/\overline{w}$	
$\overline{w}$	mean velocity	$m \cdot s^{-1}$

Greek symbols

α	curvature angle	
α, β, γ	metric tensor components	
γ	aspect ratio, $\gamma = a/b$	
Γ	diffusion coefficient	
ϕ	generic variable	
ξ, η	coordinates in the transformed plane	
μ	viscosity	$kg \cdot m^{-1} \cdot s^{-1}$
θ	dimensionless temperature, $\theta = (T - T_s)/(\overline{T} - T_s)$	

Subscripts

nb	neighbour nodal point
p	central nodal point
s	surface
k	iteration
i, j	nodal point indices

1. INTRODUCTION

The flow in curved ducts has several applications in engineering, such as in fluid transport, heat exchangers, cooling systems, refrigeration and air conditioning systems, turbomachinery, not to mention applications in other areas, such as blood flow in veins and arteries. Ducts of elliptical and rectangular cross section are usual in air conditioning systems. The main feature of the flow in curved ducts is the presence of a secondary flow as a double spiral, produced by the centrifugal force of the axial flow. This secondary flow increases the pressure drop and the heat transfer coefficient.

The first solution of the flow in curves was suggested by Dean [1], who showed that the centrifugal effect dislocates the peak of the main velocity to the external side of the curve and results in a secondary flow as a double spiral. This secondary flow is explained by the pressure gradient in the transversal cross section, induced by the centrifugal force of the main flow. This occurs due to the difference between the main velocity of the internal part of the curve, which is lower compared with the external part. Moreover, Dean [1] established a non-dimensional parameter to describe the phenomenon:

$$K = Re \sqrt{l/r_c}, \tag{1}$$

where K is the Dean number, Re the Reynolds number, l a characteristic length and r_c the curvature radius. The characteristic length l is defined as:

$$l = \sqrt{a\, b}, \tag{2}$$

where a is half of the rectangle base (or the horizontal semi-axis of ellipse) and b the half of the rectangle height (or the vertical semi-axis of the ellipse) (*figure 1*). This means that, independently of the aspect ratio, for a given value of l the areas of all the ellipses are equal. The same occurs with rectangles, but with larger area values.

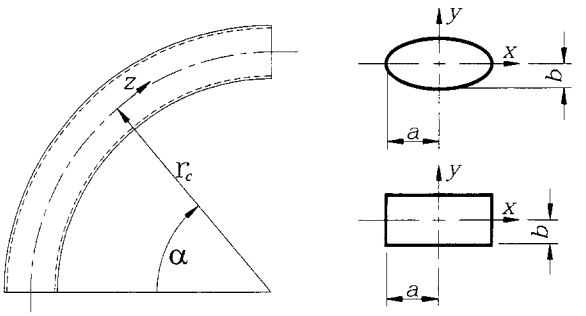

Figure 1. Problem geometry and coordinate system.

The flow in curved ducts has been studied by many authors, as suggested by Berger, Talbot and Yao [2], Nandakumar and Masliyah [3], Ito [4] and Berger [5] who reviewed the subject. The majority of these works uses toroidal coordinates system for the study of tubes with circular cross section. More recent works show the interest in the study of this kind of flow, approaching different aspects that allow to us characterise better the flow. Among these, stands out the work by Ziviani, Nieckele and Figueiredo [6] who studied the annular flow in curved tubes. Acharya, Sen and Chang [7] investigated the length of thermal entrance and the Nusselt number in helical tubes. Bolinder [8] studied the effect of the curvature and torsion in the flow in helices of rectangular cross section. Ishigaki [9] studied the flow in curved tubes with rotation. Silva, Ziviani and Valle [10] studied the heat transfer in the annular flow in curved ducts of circular cross section. Goering, Humphey and Greif [11] studied the combined effect of the curvature and body forces on the flow and heat transfer in the fully developed flow in curved tubes. Lin, Zhang and Ebadian [12] investigated the thermal and hydrodynamics entrance region in helical tubes. Wang [13] studied the combined effect of the body and centrifugal forces in the heat transfer in rectangular curved ducts with rotation. Applying the concepts of flow in curved tubes, Lynch, Waters and Pedley [14] developed a model for the blood flow in arteries, considering it as flow in tube of variable curvature.

Of particular interest to the present work, Cheng, Lin and Ou [15] studied the behaviour of the fully developed laminar flow in curved rectangular channels. Dong and Ebadian [16] studied the behaviour of the laminar flow in ducts with elliptical cross section. Silva, Valle and Ziviani [17] investigated the annular flow in ducts with elliptical cross section.

In this work, numerical results of the hydrodynamic and thermal behaviour of the flow in curved ducts with elliptical and rectangular cross section for some aspect ratios are presented. Rectangles and ellipses with aspect ratio varying between 0.7 and 1.4 and Dean number between 30 and 400 are studied. Above a Dean number of 400, the flow may become turbulent.

2. PROBLEM FORMULATION

The duct cross section (rectangular or elliptical) and the coordinate system used in the description of the problem are shown in *figure 1*. The duct curvature axis is parallel to the semi-axis b of the ellipse (side b of the rectangle), the problem being symmetrical in relation to axis x. α represents the angle in the main direction of the flow and r_c the curvature duct radio. The main direction z is linearized using $z = \alpha\, r_c$. The aspect ratio (γ) is given by the ratio of ellipse semi-axis or rectangle sides (a/b).

The pressure flow is considered as the sum of the average value in the section ($\overline{p}$) with the pressure fluctuation (p^{**}), this pressure fluctuation being independent in relation to the axial position. Defining a modified pressure that includes the gravitational effect ($p^* = p^{**} + \rho g y$) and considering only ducts with large curvature radius, the governing equations can be written as:

– mass conservation equation

$$\frac{\partial(\rho\, u)}{\partial x} + \frac{\partial(\rho\, v)}{\partial y} = 0 \tag{3}$$

– momentum equations

axial direction z

$$\frac{\partial(\rho\, u\, w)}{\partial x} + \frac{\partial(\rho\, v\, w)}{\partial y} = -\frac{\partial \overline{p}}{\partial z} + \frac{\partial}{\partial x}\left(\mu\, \frac{\partial w}{\partial x}\right) + \frac{\partial}{\partial y}\left(\mu\, \frac{\partial w}{\partial y}\right) - \frac{w}{(r_c + x)^2} \tag{4}$$

secondary direction x

$$\frac{\partial(\rho\, u\, u)}{\partial x} + \frac{\partial(\rho\, u\, v)}{\partial y} = -\frac{\partial p^*}{\partial x} + \frac{\partial}{\partial x}\left(\mu\, \frac{\partial u}{\partial x}\right) + \frac{\partial}{\partial y}\left(\mu\, \frac{\partial u}{\partial y}\right) + \frac{1}{r_c + x}\, \frac{\partial u}{\partial x} - \frac{u}{(r_c + x)^2} \tag{5}$$

secondary direction y

$$\frac{\partial(\rho\, u\, v)}{\partial x} + \frac{\partial(\rho\, v\, v)}{\partial y} = -\frac{\partial p^*}{\partial y} + \frac{\partial}{\partial x}\left(\mu\, \frac{\partial v}{\partial x}\right) + \frac{\partial}{\partial y}\left(\mu\, \frac{\partial v}{\partial y}\right) \tag{6}$$

– energy conservation equation

$$\frac{\partial(\rho\, u\, c_p\, T)}{\partial x} + \frac{\partial(\rho\, v\, c_p\, T)}{\partial y} = -\rho\, c_p\, w\, \frac{\partial T}{\partial z} + \frac{\partial}{\partial x}\left(k\, \frac{\partial T}{\partial x}\right) + \frac{\partial}{\partial y}\left(k\, \frac{\partial T}{\partial y}\right) \tag{7}$$

All equations are presented in their conservative forms, allowing a general formulation for a generic property, where these properties (μ, ρ and k) are constant.

Due to the symmetry of the problem with regard to the abscissas axis, the solution domain is reduced to half of the duct cross section. The problem boundary conditions are:

$$u = v = w = 0 \quad \text{and} \quad T = T_s$$

in the duct wall and (8)

$$v = \frac{\partial u}{\partial y} = \frac{\partial w}{\partial y} = \frac{\partial T}{\partial y} = 0$$

in the symmetry plane ($y = 0$) (9)

3. NUMERICAL METHODOLOGY

The equations (3) to (7) can be written in a generic form for a property ϕ, as:

$$\frac{\partial(\rho\, \phi)}{\partial t} + \frac{\partial(\rho\, u\, \phi)}{\partial x} + \frac{\partial(\rho\, v\, \phi)}{\partial y} = \frac{\partial}{\partial x}\left(\Gamma_\phi\, \frac{\partial \phi}{\partial x}\right) + \frac{\partial}{\partial y}\left(\Gamma_\phi\, \frac{\partial \phi}{\partial y}\right) + S_\phi \tag{10}$$

where Γ_ϕ is the property diffusion coefficient and S_ϕ the source term, data in *table I*. Despite the fact of the problem being steady, the transient term of equation (10) is used for the iterative solution of the time march process.

TABLE I
Conservation equations variables

Equation	ϕ	Γ_ϕ	S_ϕ
Continuity	1	0	0
Momentum x	u	μ	$-\frac{\partial p^*}{\partial x} + \frac{u}{(r_c + x)^2}$
Momentum y	v	μ	$-\frac{\partial p^*}{\partial y}$
Momentum z	w	μ	$-\frac{\partial \overline{p}}{\partial z} - \frac{w}{(r_c + x)^2}$
Energy	T	$\frac{k}{c_p}$	$-\rho\, w\, \frac{\partial T}{\partial z}$

In the boundary fitted coordinates system approach, the equations are solved in a transformed or computational fixed plane, independently of the geometric form. *Figures 2(a)* and *(b)* show the grids of the rectangle and ellipse in the physical domain, respectively. The equations, however, are solved in the transformed plane (ξ,η) as shown in *figure 2(c)*. The coordinate conversion of equation (10) results in the following equation:

$$\frac{\partial(\rho\,\phi)}{\partial t}+\frac{\partial(\rho\,U\,\phi)}{\partial \xi}+\frac{\partial(\rho\,V\,\phi)}{\partial \eta}= \frac{\partial}{\partial \xi}\left(\Gamma_\phi\,J\,\alpha\,\frac{\partial \phi}{\partial \xi}-\Gamma_\phi\,J\,\beta\,\frac{\partial \phi}{\partial \eta}\right) +\frac{\partial}{\partial \eta}\left(\Gamma_\phi\,J\,\gamma\,\frac{\partial \phi}{\partial \eta}-\Gamma_\phi\,J\,\beta\,\frac{\partial \phi}{\partial \xi}\right)+\widehat{S}, \quad (11)$$

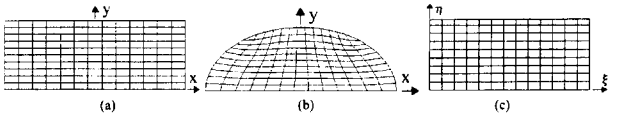

Figure 2. a, b. Physical domain. **c.** Computational domain.

where J is the transformation Jacobian, α, β and γ are the metric tensor components, U and V the contravariant components of velocity and $\widehat{S}$ the source term. The general transformation and definition of these parameters are given in Maliska [18].

The general transformed equation (10) is discretized according to the finite volume method in a boundary fitted coordinate system using a staggered grid, WUDS (Weighted Upstream Differencing Scheme) interpolation scheme and coupling pressure-velocity in the traverse plan with the SIMPLEC algorithm (Semi-Implicit Method for Pressure Linked Equations – Consistent). The coupling pressure-velocity in the axial direction was obtained by a similar procedure. The discretized equation is given by:

$$a_p\,\phi_p=\sum a_{\rm nb}\,\phi_{\rm nb}+b \quad (12)$$

where p refers to the grid point where the equation is solved, nb to its neighbours and b is the linearized source term. The coefficients a_p and $a_{\rm nb}$ and the source term b are given by Valle [19]. The problem boundary conditions are implemented using fictitious control volumes, according to the methodology presented by Maliska [18].

The velocity, pressure and temperature fields are obtained. They are the parameters used in the phenomenon analysis. For the convergence of the problem the following criterion was defined, for both velocity and temperature:

$$\mathrm{MAX}\left[\frac{|\phi^k_{i,j}-\phi^{k-1}_{i,j}|}{|\phi^k_{i,j}|}\right]<10^{-8}, \quad (13)$$

where the function MAX[ ] finds the maximum value in the domain, the subscript k represents the k-th iteration, the subscripts i and j the mesh points and the symbol || is the absolute value.

3.1. Problem validation

The main velocity experimental profiles established by Dong and Ebadian [16] were used for the validation of the numerical results, as shown in *figure 3*. As can be seen in this figure, the proposed model can reproduce the experimental results with a maximum error of 8 %. This difference is acceptable if the uncertainty of the experimental results is taken into account.

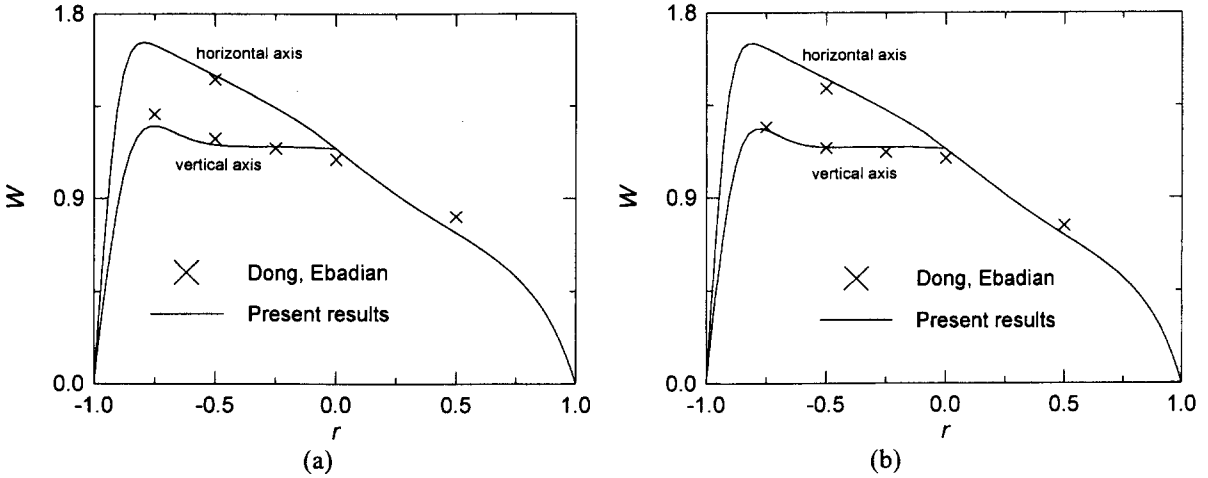

Figure 3. Dimensionless axial velocity W in the elliptic curved duct with $\gamma = 1.25$ and **(a)** $K = 441$ and **(b)** $K = 543$.

3.2. Grid test

Results were obtained for grids of 45 × 27, 50 × 30 and 55 × 33 points in directions θ and r, respectively, for a elliptic cross section. For the rectangular cross section grids of 55 × 34, 60 × 37 and 65 × 40 points in directions x and y, respectively, were analysed (*table II*). It can be observed that the pressure drop ($f\ Re$) is less sensitive to the grid refinement than the heat transfer coefficient (Nu). This fact implies that, for the analysed grids, the velocity profiles were not considerably affected by the refinement. Besides, for small Dean numbers the sensitivity to the grid refinement is even smaller for both parameters. The difference among the Nusselt number with the meshes 50 × 30 and 55 × 33, in the elliptic cross section, is of 0.7 % for $K = 400$. In the rectangular one, with the meshes 60 × 37 and 65 × 40, the difference is of 1.2 % for $K = 400$. Therefore, the meshes of 50 × 30 points for the elliptic cross section and of 60 × 37 for the rectangular one were selected.

TABLE II
Grid test

Ellipse						
K	200			400		
grid	45 × 27	50 × 30	55 × 33	45 × 27	50 × 30	55 × 33
$f\ Re$	127	127	127	162	163	163
Nu	19.0	18.8	18.7	28.1	27.6	27.4
Rectangle						
K	200			400		
grid	55 × 34	60 × 37	65 × 40	55 × 34	60 × 37	65 × 40
$f\ Re$	71.4	71.4	71.3	101	101	101
Nu	11.1	10.9	10.8	17.5	17.1	16.9

4. RESULTS AND DISCUSSION

The numerical findings allow us to analyse two aspects of the flow and heat transfer behaviour: the geometry effect (duct cross section and aspect ratio) and the Dean number effect. In *figures 4* to *9* the streamlines of the main (a) and secondary flow (b) and the isotherms (c) for three Dean number values for each geometry are presented. In these figures, the curve external side is always on the left side. Graphs showing the friction factor (*figures 10* and *12*) and Nusselt number (*figures 11* and *13*) behaviours as a function of Dean number are also presented. For each duct cross section (ellipse or rectangle) results are presented for three aspect ratio values.

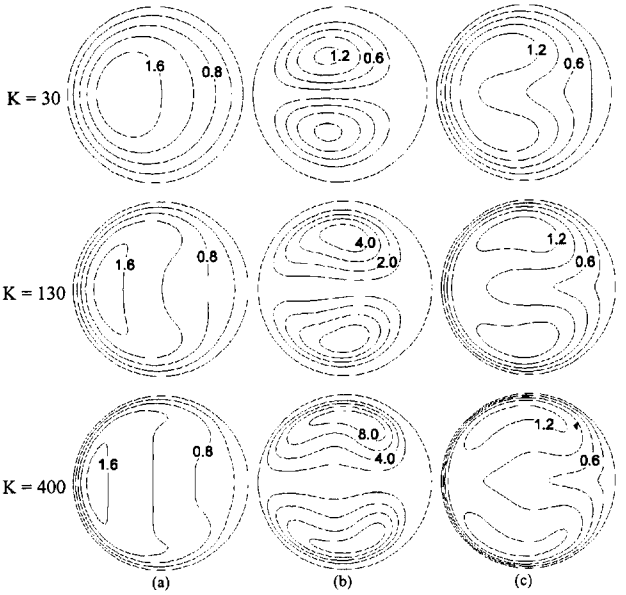

Figure 4. a. Dimensionless axial velocity W. **b.** Streamlines of secondary flow ($\times 10^{-5}$). **c.** dimensionless temperature θ for ellipse with $\gamma = 1.0$.

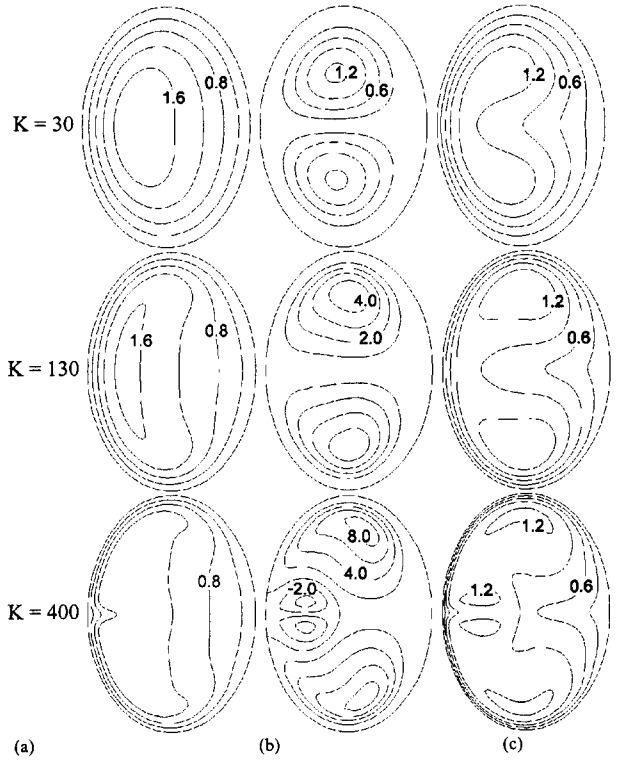

Figure 5. a. Dimensionless axial velocity W. **b.** Streamlines of secondary flow ($\times 10^{-5}$). **c.** Dimensionless temperature θ for ellipse with $\gamma = 0.7$.

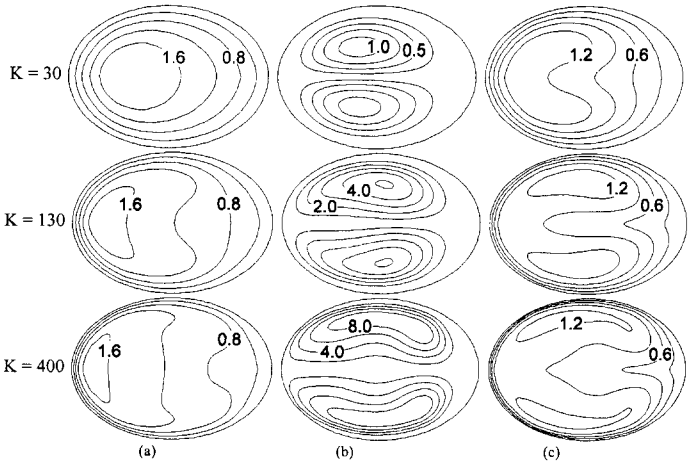

Figure 6. a. Dimensionless axial velocity W. **b.** Streamlines of secondary flow ($\times 10^{-5}$). **c.** Dimensionless temperature θ for ellipse with $\gamma = 1.4$.

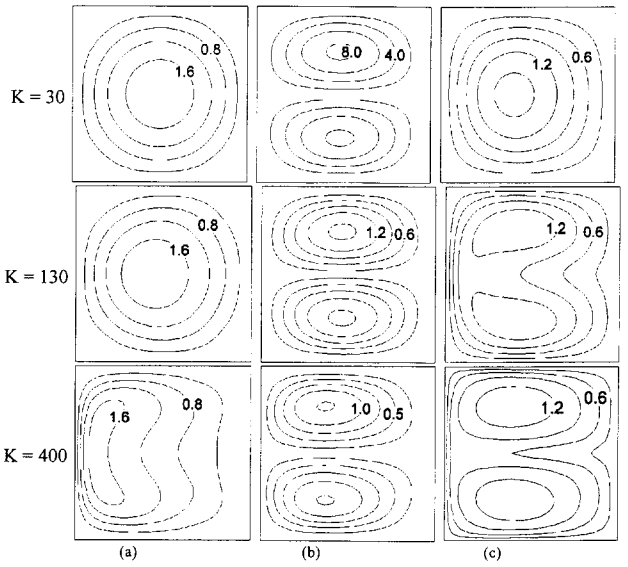

Figure 7. a. Dimensionless axial velocity W. **b.** Streamlines of secondary flow ($\times 10^{-7}$ for $K = 30$, $\times 10^{-6}$ for $K = 130$, $\times 10^{-5}$ for $K = 400$). **c.** Dimensionless temperature θ for rectangle with $\gamma = 1.0$.

4.1. Dean number effects

Firstly, the Dean number effect on the flow and heat transfer in the ellipse and rectangle with $\gamma = 1$, that is, a circle and a square, are analysed. The Dean number increase leads to a displacement of the point of the maximum axial velocity to the external side of the curve, as observed in *figure 4a* for the circle. A similar behaviour is observed for the square duct (*figure 7a*).

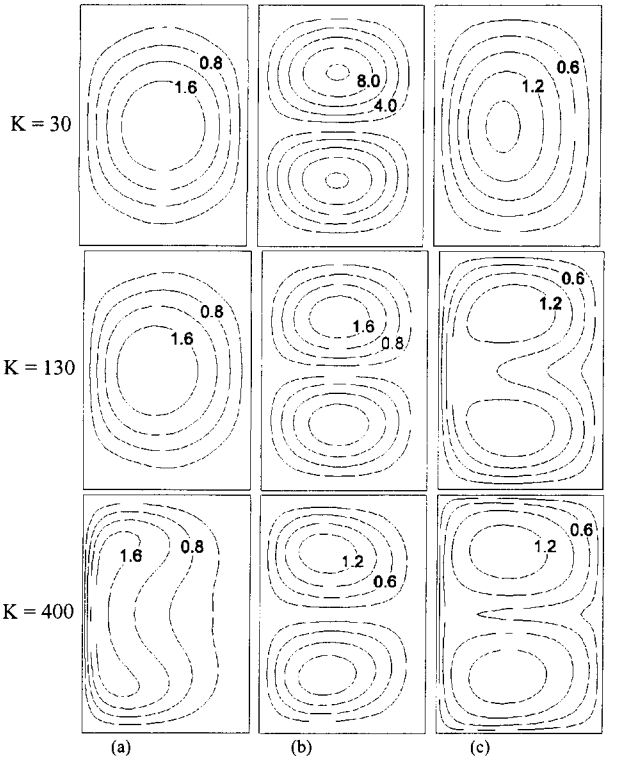

Figure 8. a. Dimensionless axial velocity W. **b.** streamlines of secondary flow ($\times 10^{-7}$ for $K = 30$, $\times 10^{-6}$ for $K = 130$, $\times 10^{-5}$ for $K = 400$) and **(c)** dimensionless temperature, θ, for rectangle with $\gamma = 0.7$.

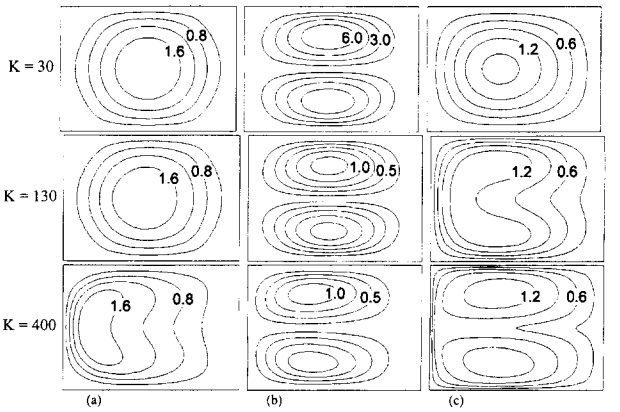

Figure 9. a. Dimensionless axial velocity W. **b.** streamlines of secondary flow ($\times 10^{-7}$ for $K = 30$, $\times 10^{-6}$ for $K = 130$, $\times 10^{-5}$ for $K = 400$). **c.** dimensionless temperature θ for rectangle with $\gamma = 1.4$.

With the largest transverse velocity gradient close to the symmetry line, the secondary flow is intensified in the circumference (*figure 4b*), as indicated by the streamlines values. In the square (*figure 7b*), despite

the form the streamlines being similar in all cases, the increase of the secondary flow is more accentuated, as can be seen by the streamlines values.

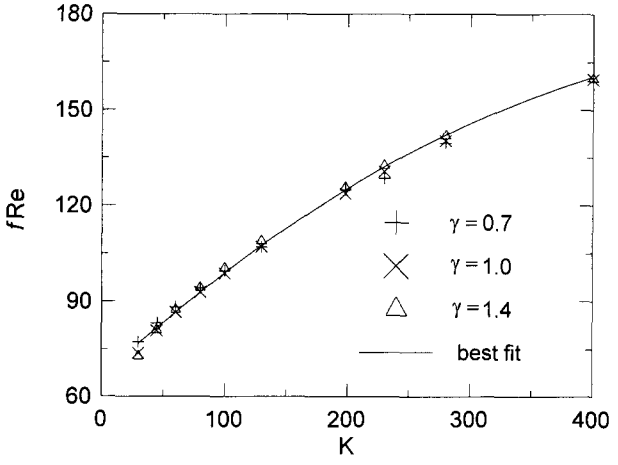

Figure 10. Friction factor versus Dean number for a duct of elliptic cross section of different aspect ratios.

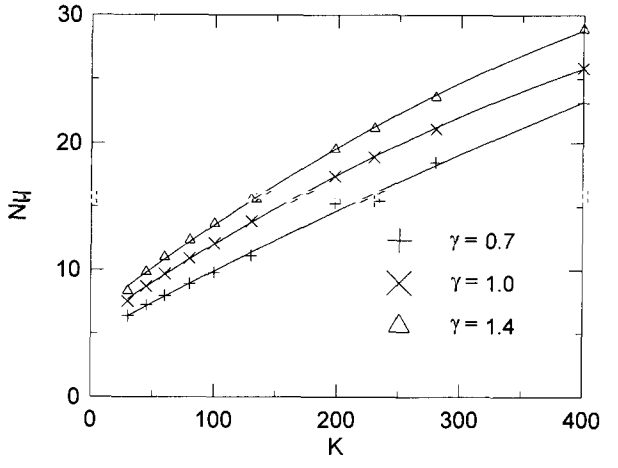

Figure 11. Nusselt number versus Dean number for a duct of elliptic cross section of different aspect ratios.

The temperature profile is strongly influenced by the secondary flow, see *figure 4c* for the circle. Due the fact that the secondary flow is less intense in the square cross section ducts, the temperature profile changes from one affected mainly by the main flow, $K = 30$ in *figure 7c*, to another where the major influence is the secondary flow, $K = 130$ and 400 in *figure 7c*.

4.2. Aspect ratio effect

Similar streamlines and isotherms behaviours are observed when the aspect ratio is different from unity.

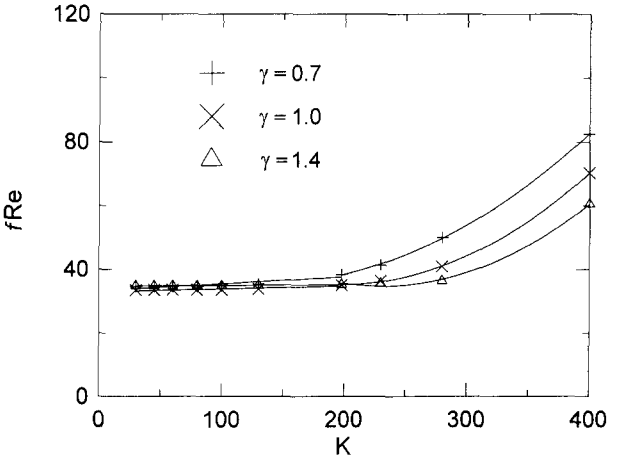

Figure 12. Friction factor versus Dean number for a duct of rectangular cross section of different aspect ratios.

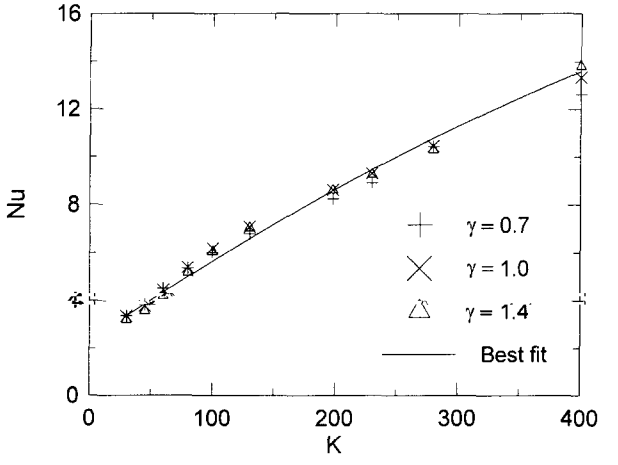

Figure 13. Nusselt number versus Dean number for a duct of rectangular cross section of different aspect ratios.

In *figure 6*, it is observed that the behaviour of both flow and temperature, in the ellipses with $\gamma = 1.4$ is very similar to that with $\gamma = 1$, as already observed by Dong and Ebadian [16] in their study of the flow in ellipses with $\gamma > 1$, see *figure 4*. In contrast, for $\gamma < 1$ the flow becomes less stable and, with the Dean number increase, there is a tendency for the formation of multiple vortices in the secondary flow; for $\gamma = 0.7$ it appears when $K = 400$, as seen in *figure 5*. This effect is due to the narrowing of the cross section in the symmetry line, moving the fluid to the superior and inferior extremities of the duct cross section.

In rectangles, the velocity and temperature behaviour is similar to that observed in the square in the cases where $\gamma > 1$ and $\gamma < 1$ (*figures 8* and *9*). Multiple vortices do not occur in the range studied. The reason for that is the used definition of characteristic length l

(equation (2)) where the rectangle area is always larger than the ellipse, for the same characteristic length. Even when the narrowing of the symmetry line is the same as for the ellipse, in the rectangle the fluid finds a larger area to dislocate from the symmetry line. Thus, the formation of multiple vortices will occur for larger Dean numbers in the rectangle.

With an increase in the aspect ratio (γ) it is possible to note that the vortices move away from the duct wall; therefore, the flow area around the vortex increases, decreasing the secondary velocities, resulting in a decrease of the heat transfer coefficient. On the other hand, it seems that the appearance of another vortices would increase the local convective coefficient; however, the mean convective coefficient does not increase, probably because these vortices are of low intensity and the affected area of the duct wall is relatively small.

4.3. Friction factor and Nusselt number

In the ellipse the pressure drop increases with Dean number (*figure 10*). Despite the change in the pattern of the secondary flow with the Dean number increase for different aspect ratios (*figures 4b* to *6b*), even with the formation of new vortices, $K = 400$ in *figure 5b*, this is not reflected in the pressure drop, represented by the friction factor in *figure 10*, which presents a similar behaviour for the different aspect ratios studied. The pressure drop is influenced mainly by the axial flow, and therefore, large changes in the secondary flow do not affect the friction factor for the different aspect ratios studied.

The differences listed in *table III* and the aspect of *figure 10* confirm the previous observations. They suggest that the aspect ratio is not an important factor in the behaviour of the pressure drop when related

TABLE III
Pressure drop versus K and γ for the elliptic cross section

K	$\gamma = 0.7$	$\gamma = 1.0$	$\gamma = 1.4$	% maximum
30	77.2	73.7	72.7	5.8
45	83.1	80.8	81.0	2.8
60	88.2	86.4	87.3	2.0
80	94.1	92.8	94.2	1.6
100	99.4	98.7	100.3	1.7
130	106.9	106.9	108.8	1.8
200	124.9	123.7	125.7	1.6
230	128.5	130.6	132.5	3.1
280	139.5	140.3	141.9	1.7
400	159.0	159.5	159.8	0.5

TABLE IV
Maximum secondary velocity for the elliptic ducts

K	$\gamma = 0.7$	$\gamma = 1.0$	$\gamma = 1.4$
30	$3.61 \cdot 10^{-4}$	$4.60 \cdot 10^{-4}$	$5.00 \cdot 10^{-4}$
130	$2.05 \cdot 10^{-3}$	$2.22 \cdot 10^{-3}$	$2.47 \cdot 10^{-3}$
400	$5.91 \cdot 10^{-3}$	$6.71 \cdot 10^{-3}$	$7.47 \cdot 10^{-3}$

TABLE V
Constants in equation $Nu = f(K)$ for the elliptic ducts

γ	0.7	1.0	1.4
a	$-5.0 \cdot 10^{-5}$	$-4.3 \cdot 10^{-5}$	$-1.8 \cdot 10^{-5}$
b	$7.6 \cdot 10^{-2}$	$6.8 \cdot 10^{-2}$	$5.3 \cdot 10^{-2}$
c	6.5	5.7	4.8

TABLE VI
Constants in equation $f\ \mathrm{Re} = f(K)$ for the rectangular ducts

γ	0.7	1.0	1.4
a	$6.54 \cdot 10^{-4}$	$8.5 \cdot 10^{-4}$	$9.06 \cdot 10^{-4}$
b	−0.17	−0.335	−0.419
c	46.6	68.1	83.1

TABLE VII
Nusselt number versus Dean and γ for the rectangular ducts

K	$\gamma = 0.7$	$\gamma = 1.0$	$\gamma = 1.4$	% maximum
30	3.39	3.37	3.21	5.3
45	3.87	3.81	3.59	7.1
60	4.57	4.49	4.24	7.3
80	5.46	5.47	5.24	4.3
100	6.18	6.30	6.14	2.6
130	7.08	7.30	7.21	3.2
200	8.93	9.20	9.06	3.0
230	9.82	10.1	9.88	2.5
280	11.3	11.5	11.2	2.4
400	14.6	15.1	14.8	2.9

to the Dean number. Within the Dean number and aspect ratio ranges studied, the pressure drop can be expressed as a function of Dean number by the following expression:

$$f\ Re = 3.1 \cdot 10^{-4}\ K^2 + 0.36\ K + 66.0 \qquad (14)$$

The heat transfer, represented by the Nusselt number, also increases with the Dean number (*figure 11*). The heat transfer, unlike the pressure drop, is essentially affected by the secondary flow. The narrowing of the section in the symmetry line, due the decrease in the aspect ratio, reduces the effect of the centrifugal force, turning the secondary flow less intense and less stable. This reduction in the intensity of the secondary flow reduces the heat transfer, producing smaller Nusselt numbers for small aspect ratios, as seem in *figure 11*. The streamlines in *figures 4*, *5*, and *6* do not show these effects, but an analysis of the fields of secondary flow when the aspect ratio decrease from 1.4 to 0.7 indicates a reduction from 20 to 38 % in the maximum velocities, depending on the Dean number, as shown in *table IV*.

The heat transfer can be obtained by a general expression like:

$$Nu = a\ K^2 + b\ K + c \qquad (15)$$

where the values of the constants a, b and c, for the different aspect ratios, are presented in the *table V*.

In the duct with rectangular cross section, the main flow varies slightly for a Dean number up to 130 for different geometries, $K = 30$ and 130 in *figures 7(a)* to *9(a)*. The pressure drop is almost constant in that range, *figure 12*. Additionally $f\ Re$ can be considered constant and equal to 34.8, 33.7 and 34.9 for aspect ratios of 0.7, 1.0 and 1.4, respectively. Therefore, it can be assumed that:

$$f\ Re = 34.5 \text{ for } 30 < K < 130. \qquad (16)$$

When the Dean number increases beyond this value, the displacement of the main velocity maximum to near the wall increases the velocity gradient, for all geometries studied. Those larger velocity gradients near the wall are responsible for the increase in the friction factor (*figure 12*). Due to the aspect ratio increase, the larger velocity gradients and the face area where it occurs decrease, $K = 400$ in *figures 7a* to *9a*, also decreasing the pressure drop, (*figure 12*). A general expression for the pressure drop as a function of the Dean number for this case can be given as:

$$f\ Re = a\,K^2 + b\,K + c \text{ for } K > 130 \qquad (17)$$

where a, b and c depend on the aspect ratio and they are presented in the *table VI*.

For ducts with rectangular cross section the heat transfer is a function only of the Dean number (*figure 13*). In the studied limits of Dean number, the aspect ratio does not affect either the secondary flow (*figures 7b* to *9b*), or the heat transfer (*figure 13*). This can be verified in *table VII*. The variation of the Nusselt number as a function of the Dean number for the flow in ducts of rectangular cross section, in the considered Dean number and aspect ratio ranges, can be represented by the equation:

$$Nu = -1.71 \cdot 10^{-5}\ K^2 + 3.5 \cdot 10^{-2}\ K + 2.31 \qquad (18)$$

5. CONCLUSIONS

The laminar flow in curved ducts, during steady, incompressible and fully developed flow, is studied by numerically, solving the conservation equations of movement and energy. Results are obtained for Dean number values between 30 and 400 and different cross sections (ellipses or rectangles) with aspect ratios between 0.7 and 1.4. The main and secondary velocity and temperature profiles are analysed beyond the pressure drop and heat transfer.

For the flow in curved ducts, the Dean number increase dislocates the point of maximum axial velocity for the most external region of the curve, intensifying the secondary flow.

The displacement of the axial velocity leads to a pressure drop increase, while the secondary flow increase intensifies the heat transfer in all cross sections studied.

The velocities and temperature behaviour for the flow in ducts with elliptical cross section with $\gamma > 1$ is similar to the flow in ducts of circular section, up to the limit of $\gamma = 1.4$, i.e., the streamlines and isotherms forms. In contrast, for $\gamma < 1$ the flow becomes less stable with the Dean number increase and multiple vortices are formed for $\gamma = 0.7$ and $K = 400$.

For the flow in tubes of rectangular cross section the behaviour changes slightly when compared to the square cross section, for both $\gamma > 1$ and $\gamma < 1$, in the studied limits. With that geometry the multiple vortices formation does not occur, presenting a larger limit of stability than in the elliptic configurations.

In the elliptic geometry, the pressure drop increases with the Dean number in all cases. Within this range, the aspect ratio does not influence the pressure drop, since it depends mainly on the main flow, not being affected by the secondary flow multiple vortices. The heat transfer also increases with the Dean number and, in contrast to the friction factor, it is strongly affected by the aspect ratio, which affects the secondary flow.

In the ducts of rectangular cross section the pressure drop remains constant within the Dean number range, while the main flow does not alter significantly. After this point, it has a considerable growth, strongly influenced by the aspect ratio. The heat transfer also increases with the Dean number. However, as the aspect ratio does not affect the secondary flow significantly, it does not present marked variations on the heat transfer.

A larger pressure drop is observed for the elliptic duct due to the appearance of a more intense secondary flow for that geometry.

The heat transfer also is larger for the elliptical geometry because the secondary flow is more intense, in the limits studied.

REFERENCES

[1] Dean W.R., The streamline motion of fluid in a curved pipe, Philos. Mag. 30 (1928) 673–695.

[2] Berger S.A., Talbot L., Yao L.S., Flow in curved pipes, Ann. Rev. Fluid Mechanics 15 (1983) 461–512.

[3] Nandakumar K., Masliyah J.H., Swirling flow and heat transfer in coiled and twisted pipes, in: Advances in Transfer Processes, Wiley Eastern, vol. 4, 1986, pp. 49–112.

[4] Ito H., Flow in curved pipes, JMSE Int. J. 30 (1987) 543–552

[5] Berger S.A., Flow and heat transfer in curved pipes and tubes, AIAA Paper, 91–0030, 1991.

[6] Ziviani M., Nieckele A.O., Figueiredo A.M.D., Escoamento anular de dois líquidos imiscíveis em tubos curvos, in: Proceedings of IV Encontro Nacional de Ciências Térmicas, Rio de Janeiro, Brazil, 1992, pp. 171–174.

[7] Acharya N., Sen M., Chang H.C., Thermal entrance and Nusselt numbers in coiled tubes, Int. J. Heat Mass Tran. 37 (1994) 336–340.

[8] Bolinder C.J., First- and higher-order effects of curvature and torsion on the flow in a helical rectangular duct, J. Fluid Mech. 314 (1996) 113–138.

[9] Ishigaki H., Laminar flow in rotating curved pipes, J. Fluid Mech. 329 (1996) 373–388.

[10] Silva R.J., Valle R.M., Ziviani M., Análise hidrodinâmica do escoamento anular de dois líquidos imiscíveis em tubos elípticos curvos, in: Proceedings of III Congreso Iberoamericano de Inginiería Mecánica, Havana, Cuba, 1997 (CD-ROM).

[11] Goering D.J., Humphey J.A.C., Greif R., The dual influence of curvature and buoyancy in fully developed tube flows, Int. J. Heat Mass Tran. 40 (1997) 2187–2199.

[12] Lin C.X., Zhang P., Ebadian M.A., Laminar forced convection in the entrance region of helical pipes, Int. J. Heat Mass Tran. 40 (1997) 3293–3304.

[13] Wang L., Buoyancy-force-driven transitions in flow structures and their effects on heat transfer in a rotating curved channel, Int. J. Heat Mass Tran. 40 (1997) 233–235.

[14] Lynch D.G., Waters S.L., Pedley T.J., Flow in a tube with non-uniform, time- dependent curvature: governing equations and simple examples, J. Fluid Mech. 323 (1996) 237–265.

[15] Cheng K.C., Lin R.C., Ou J.W., Fully developed laminar flow in curved rectangular channels, J. Fluid Eng. (3) (1976) 41–48.

[16] Dong Z.F., Ebadian M.A., Numerical analysis of laminar flow in curved elliptic ducts, J. Fluid Eng. 113 (1991) 555–562.

[17] Silva R.J., Ziviani M., Valle R.M., Transferência de calor no escoamento anular desenvolvido de dois líquidos imiscíveis em tubos curvos, in: Proceedings of VI Congresso Brasileiro de Engenharia e Ciências Térmicas / VI Congreso Latinoamericano de Transferencia de Calor y Materia, Florianópolis, Brazil, 1996, pp. 1303–1308.

[18] Maliska C.R., Transferência de calor e mecânica dos fluidos computacional, LTC Editora, Rio de Janeiro, 1995.

[19] Valle R.M., Escoamento laminar em placas de orifício. Análise teórica e experimental em regime permanente e transiente, Thesis, Universidade Federal de Santa Catarina, Brazil, 1995.